1 CFD Test Cases

1.1 Test Case 1 Laminar Oil Transport in a Pipeline

1.1.1 Case Description

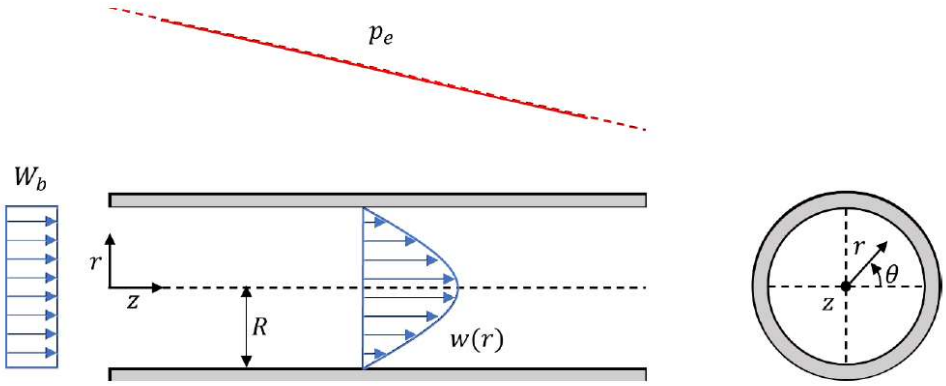

Fig. 1. Sketch of the case

The test case considers laminar oil flow in a pipeline, as illustrated in figure 1. The steady-state Navier–Stokes equations are solved using a 2D axisymmetric domain shaped as a circular sector, shown in figure 2, which exploits the symmetry of the problem. At the inlet, a uniform axial velocity equal to the bulk velocity W_b is imposed, while the radial and tangential velocity components are set to zero. At the outlet, the excess pressure is prescribed, typically set to zero. The pipe walls are modeled as stationary with a no-slip condition, enforcing zero fluid velocity at the boundaries.

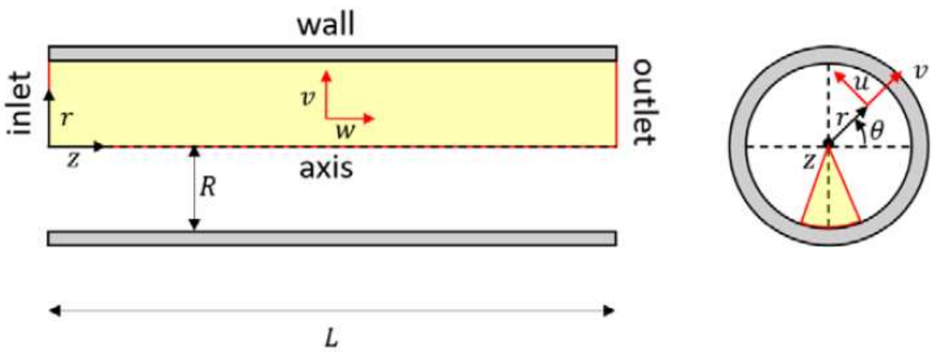

Fig. 2. Domain and boundary conditions

1.1.2 Input Data

The input data for the simulation are provided in Table 1. The Reynolds number, calculated using Eq. 10, is less than 2000, confirming that the flow is laminar.

$$Re_b = \frac{W_b D}{\nu} = \frac{0.45 \times 0.15}{3.5 \times 10^{-4}} = 192.86 < 2000 \tag{1}$$

Parameter	Value
Pipe Diameter D	$0.15m$
Bulk Velocity W_b	$0.45m/s$
Fluid Density ρ	$910Kg/m^3$
Kinematic Viscosity ν	$3.5 \times 10^{-4}m^2/s$
Pipe Length L	$3m$

Table 1. Input Data

1.1.3 Entrance Length

Different formulas for fully developed length are reported in the literature because developing length is sensitive to the inlet conditions and the pipe geometry. Two proposed equations for the entrance length in a circular pipe under laminar flow conditions are given in Eq. 2 and Eq. 3. To verify that fully developed flow conditions are satisfied, the velocity profile is monitored at axial distances of 0.5, 1.0, 1.45, 1.65, and 2.0 m from the flow entrance, as shown in figure 3. It is evident that the velocity profile progressively develops into a parabolic shape along the axial direction. Beyond 1.45 m, the velocity profile shows negligible variation, indicating that the flow has reached a fully developed state. Moreover, the wall shear stress is monitored at the same locations and is observed to become nearly constant beyond 1.45 m, as shown in figure 4.

$$L_e = 0.05Re \times D = 0.05 \times 193 \times 0.15 = 1.45m \tag{2}$$

$$L_e = 0.057Re \times D = 0.057 \times 193 \times 0.15 = 1.65m \tag{3}$$

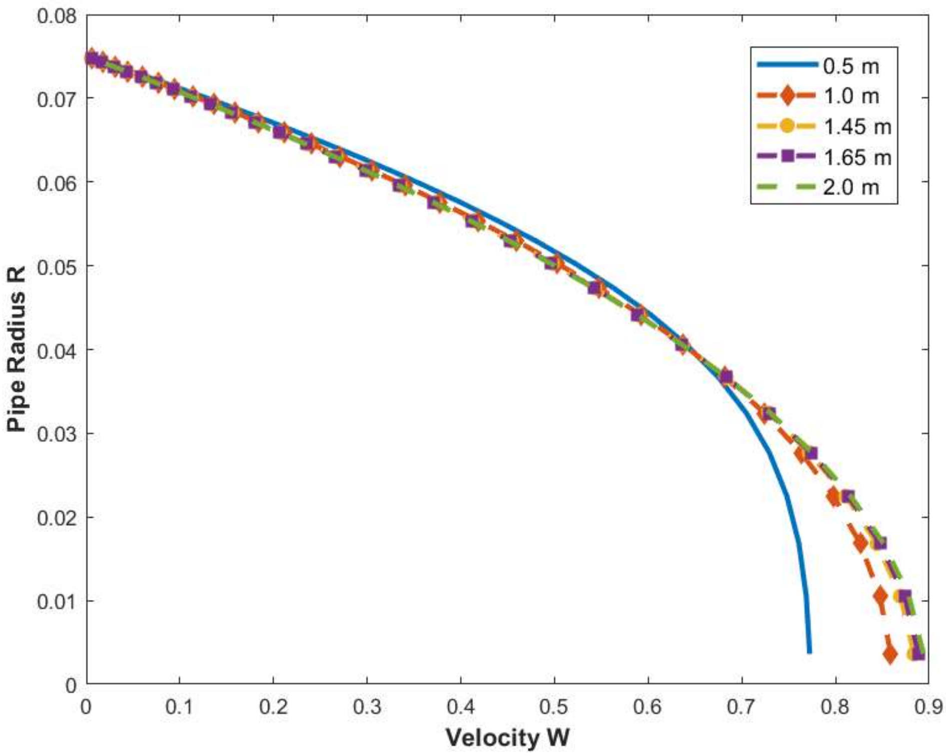

Fig. 3. Velocity (W) profile at 0.5, 1.0, 1.45, 1.65 and 2.0 m

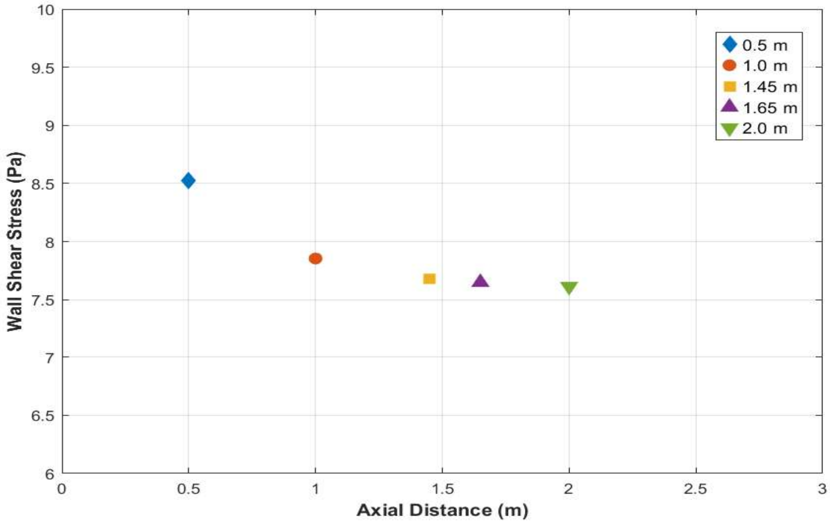

Fig. 4. Wall Shear Stress at 0.5, 1.0, 1.45, 1.65 and 2.0 m

1.1.4 Numerical Simulation

The simulation was performed using a mesh consisting of 300 cells along the axial (Z) direction and 30 cells in the radial direction, with a power-law ratio of -1.1 to refine the mesh near the pipe wall. Figures 5 and 6 show the velocity and pressure contours along the pipe, respectively. The results appear physically consistent. After the entrance length, the velocity profile becomes parabolic, with a maximum at the center of the pipe that is approximately twice the bulk velocity, and zero velocity at the pipe wall, in accordance with the no-slip boundary condition. The pressure decreases monotonically along the pipe, as expected, since the pressure gradient is the primary driving force of the flow.

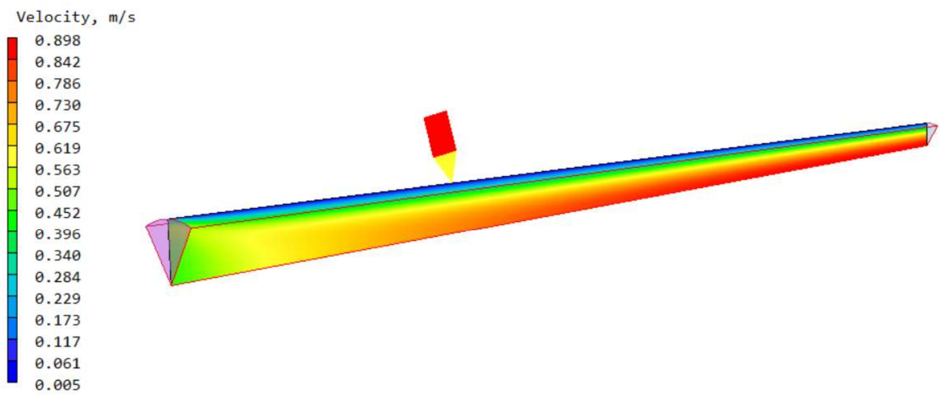

Fig. 5. Velocity Contour

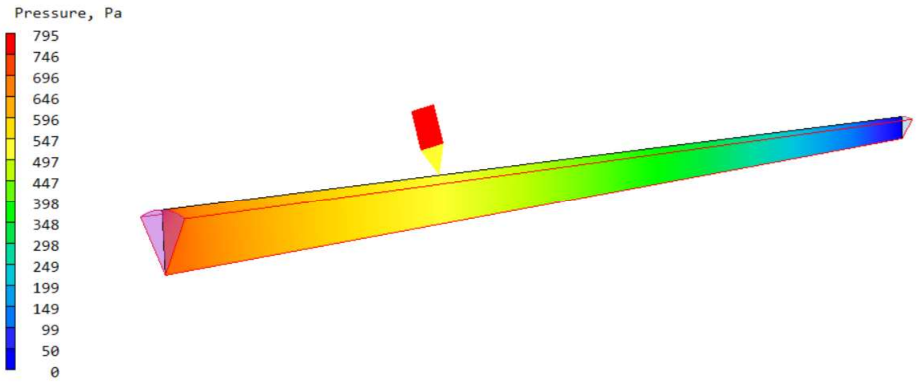

Fig. 6. Pressure Contour

1.1.5 Numerical Convergence and Grid Independence

To ensure numerical convergence of the algorithm, the normalized residuals of pressure, radial velocity and axial velocity are monitored and the solution is considered converged once all residuals fall below 1×10^{-3}, as shown in Figure 7.

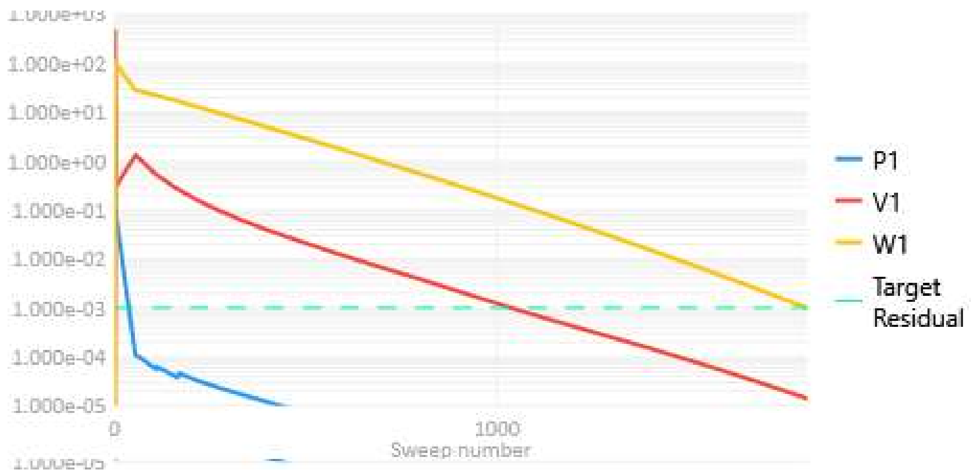

Fig. 7. Residuals

To assess the discretization error, four meshes, listed in Table 2, were considered. The wall shear stress along with pressure and velocity values at the pipe centerline and at an axial location of 2.0 m from the inlet were monitored, as shown in Figure 8. The variations are within acceptable limits for the three finest meshes. In addition, the velocity profile at 2.0 m from the inlet is presented in Figure 9, where the profiles obtained using the different meshes overlap, confirming grid independence.

Mesh	Elements in Radial Direction	Elements in axial Direction
Mesh 1	10	100
Mesh 2	20	200
Mesh 3 (Main Mesh)	30	300
Mesh 4	40	400

Table 2. Mesh Data

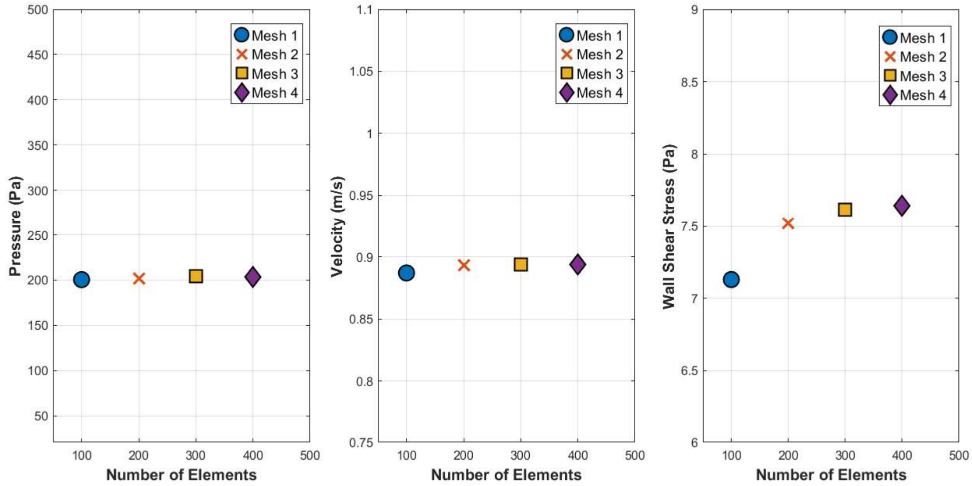

Fig. 8. Pressure, Velocity and Wall Shear Stress values at distance 2.0m from inlet for the 4 meshes

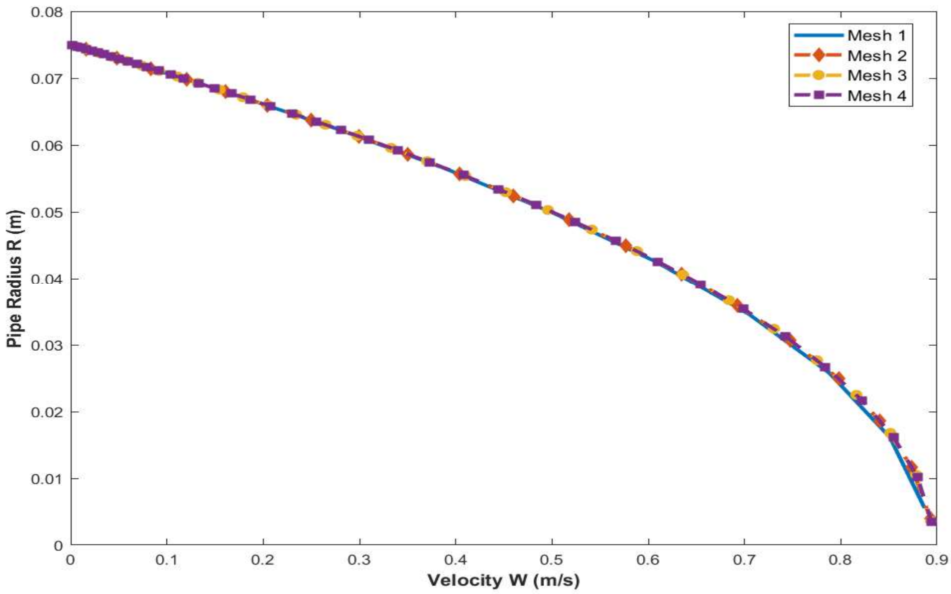

Fig. 9. Velocity profile at distance 2.0m from inlet for the 4 meshes

1.1.6 Validation

The analytical solutions for the velocity, shear stress, and pressure gradient are given by Equations 4–8, which relate all quantities to the bulk velocity, a known parameter in the test case.

$$Q = \int_0^R w(r) 2\pi r dr = -\frac{\pi R^4}{8\mu}\frac{dp_e}{dz} \tag{4}$$

$$W_b = \frac{Q}{\pi R^2} = -\frac{R^2}{8\mu}\frac{dp_e}{dz} \tag{5}$$

$$W(r) = 2W_b(1 - \frac{r^2}{R^2}) \tag{6}$$

$$\frac{dp_e}{dz} = -\frac{8\mu W_b}{R^2} \tag{7}$$

$$\tau_{rz} = -\mu\frac{dW}{dr} = \frac{4\mu W_b r}{R^2} \tag{8}$$

The axial velocity, shear stress, and pressure gradient are compared with the analytical solutions obtained from Equations 4–8. Figure 10 shows that the axial velocity profile from the CFD results at 2.0 m from the inlet, where the flow is fully developed, coincides with the analytical solution. Figure 11 illustrates that the pressure along the pipe axis decreases linearly, indicating a constant pressure gradient. The pressure gradient predicted by the CFD simulation is -204.5 Pa/s, in close agreement with the analytical value of -203.8 Pa/s. Figure 12 shows that the shear stress profile obtained from the CFD results closely matches the analytical profile, with the maximum shear stress occurring at the pipe wall and nearly zero shear stress at the centerline.

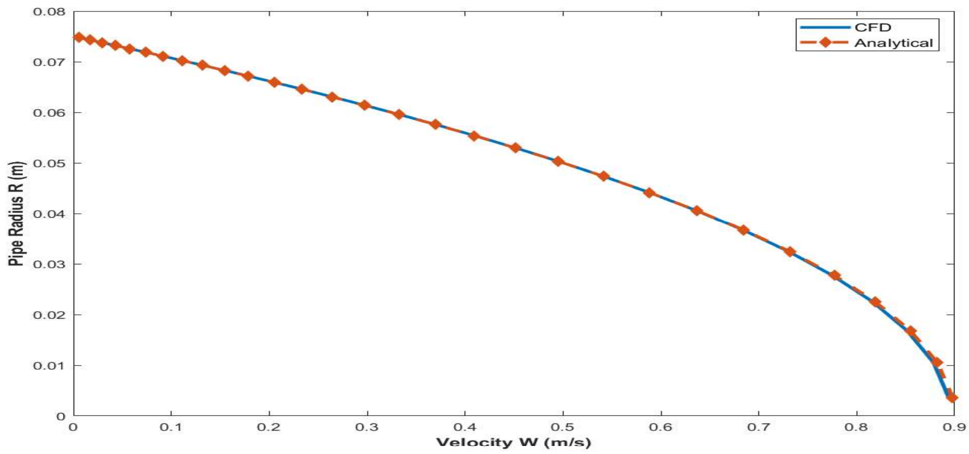

Fig. 10. Velocity profile

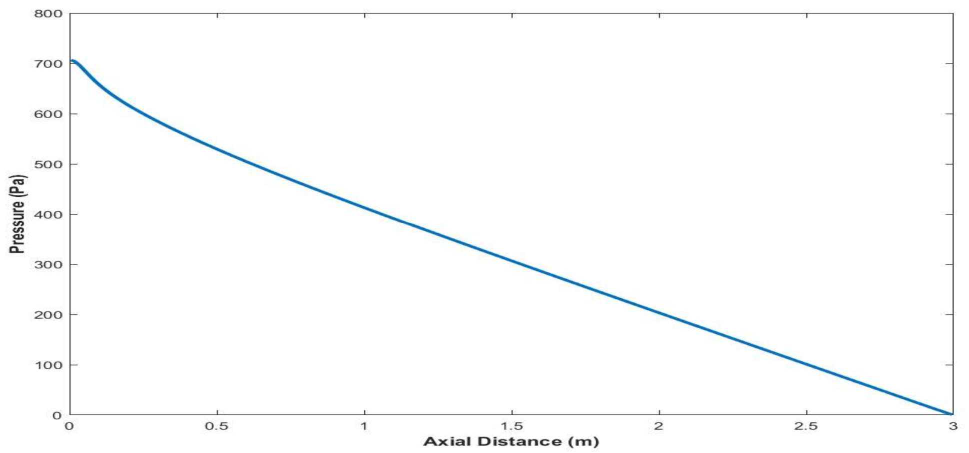

Fig. 11. Pressure profile

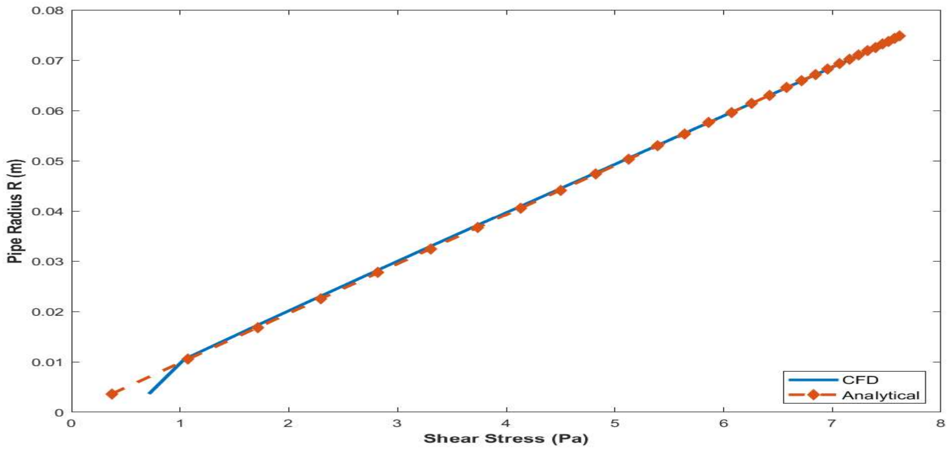

Fig. 12. Shear Stress profile

1.1.7 Friction Factor

The friction factor can be obtained from the CFD results using Equation 9, and it can also be calculated analytically using the formula $f = 64/Re$. Both methods yield a value of 0.33, indicating excellent agreement between the numerical and analytical results.

$$f = \frac{8\tau_w}{\rho W_b^2} \tag{9}$$

Figure 13 shows the friction factor values obtained at different Reynolds numbers by varying the inlet velocity, compared with the analytical values calculated using the formula $f = 64/Re$.

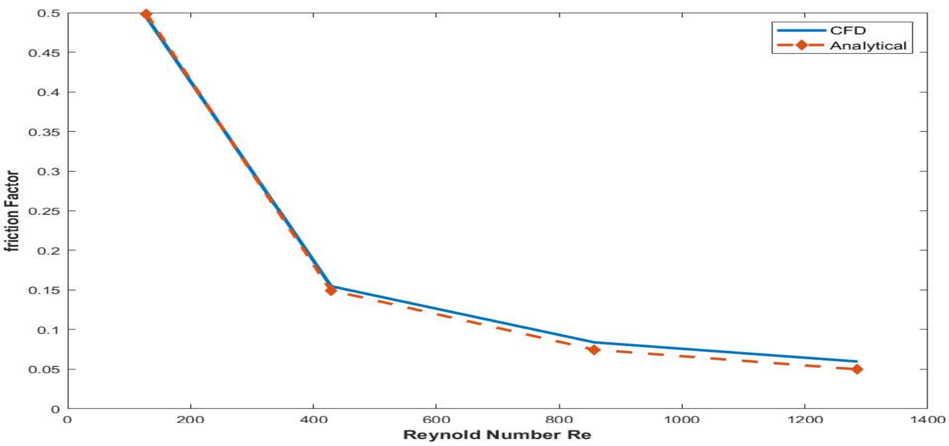

Fig. 13. Friction Factor